Journal of Integrative Neuroscience

Original Research

Network pharmacology and the experimental findings of Bushenhuoxue formula for improving hippocampal neuron injury in vascular demented rats

Shan Luo[1,†], Jiaxing Jing[1,†], Ying Zhang[2], Wentao Yu[3,4,*], Weijuan Gao[2,4,*]

[1]*The Graduate College, Hebei University of Chinese Medicine, 050091 Shijiazhuang, Hebei, China*

[2]*The Basic Medicine College, Hebei University of Chinese Medicine, 050200 Shijiazhuang, Hebei, China*

[3]*The Acupuncture and Massage College, Hebei University of Chinese Medicine, 050200 Shijiazhuang, Hebei, China*

[4]*Hebei Key Laboratory of Chinese Medicine Research on Cardio-cerebrovascular Disease, 050091 Shijiazhuang, Hebei, China*

*Correspondence: yuwentao@hebcm.edu.cn (Wentao Yu); gaoweijuan@hebcm.edu.cn (Weijuan Gao)
†These authors contributed equally.

DOI:10.31083/j.jin2004087

Submitted: 29 July 2021 Revised: 26 October 2021 Accepted: 3 November 2021 Published: 30 December 2021

We used network pharmacology to predict the correlation between the pathway of Bushenhuoxue formula in the treatment of vascular dementia and carried out experiments to verify the correlation between drug composition and disease. By screening the active components and key targets through various databases and drawing the topological network diagram, we obtained 502 effective compound targets, 601 disease targets, 95 disease-related compound targets, and 162 pathways. The pathway related to vascular dementia may be neurodegeneration-multiple diseases, PI3K-Akt signaling pathway, Mitogen-activated protein kinase signaling pathway, or HIF-1 signaling pathway. By detecting the learning and memory ability of vascular dementia rats, the morphology of the hippocampus under the electron microscope, the degree of neuronal damage, and autophagy-related proteins, the results showed that the Bushenhuoxue formula could improve the neuronal injury induced by ischemia in the hippocampus, down-regulate the level of autophagy, and thereby improve learning and memory. Therefore, the Bushenhuoxue formula may improve the ischemic injury of neurons by regulating the mechanism of neuronal autophagy.

Keywords

Autophagy; Bushenhuoxue formula; Network pharmacology; Vascular dementia

1. Introduction

Dementia is a significant public health problem worldwide. To ensure social and economic stability, many countries have promulgated relevant policies to improve the quality of care and life of patients with dementia [1]. Vascular dementia (VD) is the most severe form of vascular cognitive impairment [2]. It refers to cognitive dysfunction's clinical syndrome caused by cerebrovascular events based on brain-tissue damage [3]. It can be diagnosed by combining both clinical defects and radiographic results [4]. The molecular mechanism of the cerebrovascular disease remains unclear, and therefore the available treatment is minimal. Some studies have even shown that VD coexists in clinical patients with Alzheimer's disease; the combination often increases the difficulty of treatment [5]. VD is the only type of dementia that can be prevented by early treatment [6]. Risk factors for VD development include hyperlipidemia, hypertension, diabetes mellitus, and tobacco use. The risk of developing VD doubles with every five years of age after 65 [7].

VD has been recorded in Traditional Chinese Medicine (TCM), mainly manifested as a progressive declination of memory. TCM believed that VD's primary etiology and pathogenesis included kidney deficiency, blood stasis, and phlegm obstruction [8]. The principle of treatment is tonifying kidney and essence, promoting blood circulation, and removing blood stasis. Bushenhuoxue formula (BSHXF) consists of eight herbs, including *Polygonum Multiflorum Thunb*, *Alpinia Oxyphylla Miq*, *Juglans Regia L*, *Panax Ginseng* C. A. *Mey*, *Chuanxiong Rhizoma*, *Radix Salviae*, *Angelicae Sinensis Radix*, and *Curcuma Aromatica Salisb*. *Panax Ginseng* C. A. *Mey* is thought to help in nourishing the five viscera and calming the nerve. *Polygonum Multiflorum Thunb* is thought to enrich the blood and essence. *Juglans Regia L* is thought to nourish the kidneys and enhance the Yang. *Alpinia Oxyphylla Miq* is thought to nourish the kidney and strengthen the essence.

Chuanxiong Rhizoma and *Curcuma Aromatica Salisb* are thought to promote blood circulation and qi. *Angelicae Sinensis Radix* is thought to nourish and activate blood circulation. *Radix* Salviae is thought to promote blood circulation and remove blood stasis. These traditional Chinese medicines are thought to play a role in anti-inflammation, preventing atherosclerosis, improving learning and memory abilities, improving brain metabolic disorders, and protecting nerve cells. Clinical studies have confirmed the effectiveness of BSHXF in the treatment of VD [9], and its mechanism might be related to the regulation of the PI3K/AKT signaling pathway and reduction of hippocampal nerve cell apoptosis

[10, 11]. We found that this highly overlapped with the classic autophagy signaling pathway PI3K/Akt/mTOR [12]. Autophagy is a cellular defense mechanism produced in eukaryotic cells and plays a regulatory role in neuronal death induced by ischemia. Therefore, we speculated that autophagy is involved in the pathogenesis and prognosis of VD. However, the composition of the TCM prescription is so complex that it is difficult to fully clarify the mechanism of BSHXF through traditional research methods such as animal experiments or cell culture. Network pharmacology can effectively and systematically clarify the composition and molecular mechanism of TCM prescriptions [13]. In this study, target prediction and pathway enrichment analysis were used to explore the action targets, biological process, and main pathway of BSHXF in the treatment of VD. Subsequently, animal experiments were conducted to verify the autophagy mechanism, clarify the therapeutic mechanism of BSHXF at the molecular level, and provide new ideas and targets for clinical treatment of VD.

2. Materials and methods

2.1 Collection and screening of active components of Chinese medicines in BSHXF

Eight kinds of herbs of BSHXF were provided by Yi Ling Medicine Company (Shijiazhuang, China, Drug Manufacturing Certificate: JI20150126): *Polygonum Multiflorum Thunb* (Product batch number: B2003001); *Alpinia Oxyphylla Miq* (Product batch number: B2003001); *Juglans Regia L* (Product batch number: B1902001); *Panax Ginseng* C. A. *Mey* (Product batch number: B1912001), *Chuanxiong Rhizoma* (Product batch number: B1906002), *Radix Salviae* (Product batch number: B1909002), *Angelicae Sinensis Radix* (Product batch number: B2007001) and *Curcuma Aromatica Salisb* (Product batch number: B1902002). All herbs in BSHXF were processed conforming to the standards of Chinese Pharmacopeia 2015. The Traditional Chinese Medicine Systems Pharmacology Database (TCMSP) contains 499 herbs and the compound ingredients of each herb registered in the 2010 edition of the Chinese Pharmacopoeia; it also includes chemicals, targets, drug-target networks, and associated drug-target-disease networks. According to the usage guide of the TCMSP database [14], the standard set for bioavailability (OB value) was $\geq$30%, and drug-like property (DL) was $\geq$0.18. We used the TCMSP database to search Panax Ginseng C. A. Mey, Angelica Sinensis, Chuanxiong Rhizoma, Curcuma Aromatica Salisb, and the practical components and targets *Radix Salviae*. The active chemical components of *Polygonum Multiflorum Thunb*, *Juglans Regia L* and *Alpinia Oxyphylla Miq* were obtained from the TCMID database. We used different databases and software sources to perform this work (**Supplementary Table 1**).

2.2 Protein targets of active components

The TCMSP database contained the active components of five herbal medicines in BSHXF; the related targets of these active components were further searched and downloaded. We used the TCMID database to get the effective compounds of the other three herbal medicines. The associated targets of these herbals were obtained from the SwissTargetPrediction database [15]. We download all possible indicators under the condition of *Homo sapiens* by uploading the SMILE structural formula form for each compound, then sorted according to probability, selecting the indexes with high probability for research. Finally, we used UniProt for canonical naming.

2.3 Identification putative targets of VD

The search terms and disease genes were screened in GeneCards [16], OMIM [17], and DisGenet databases [18]. Each drug target was compared with the disease target; common targets were screened out. The R language (Version 3.6.3, Lucent Technologies, USA) and Venny 2.1 (https://bioinfogp.cnb.csic.es/tools/venny/index.html) were used to draw the Wayne diagram; these are shown as the target genes of BSHXF in the treatment of VD.

2.4 Network construction and analysis

The disease-drug gene target information was put into the STRING database to obtain the target interaction relationship. Cytoscape 3.6.0 (Version 3.6.0, National Resource for Network Biology, USA) was used to construct an optical network topology (PPI) to understand the relationship between proteins. The NetworkAnalyzer was used for network analysis. The size and degree of the nodes in the network were adjusted. The larger the graph, the greater the degree value, and the more critical the role in the network. The nodes in the network represent the targets or compounds, whereas the edges represent the associations between active components and the VD targets. According to enrichment analysis of the pathways involved in the above drug targets, the fundamental molecular mechanism of BSHXF in treating diseases was further explored, and the multi-level network correlation diagram of BSHXF-component-target was then constructed.

2.5 GO and KEGG pathway analysis

In the enrichment analysis of GO and KEGG, we used R language and Bioconductor. Bioconductor also contained many packages, such as clusterProfiler, org.Hs.eg.db, colorspace, stringi, DOSE, pathview, which can be used for more accurate prediction. A threshold value of $p \leq 0.05$ was used. The number of enriched genes sorted the top 20 genes in descending order, and then R language (Version 3.6.3, Lucent Technologies, USA) was used to create a bar plot and bubble graph. The main potential biological processes and signaling pathways by which BSHXF may act in the treatment of VD could be predicted through enrichment analysis. Finally, we use Cytoscape to create a visualized network.

2.6 Experimental animals and groups

Fifty SPF, male, Sprague Dawley rats (8 weeks, 250–280 g)were provided by the Beijing Vital River Laboratory Animal Technology Co. Ltd. (license No.: SCXK), Beijing 2016-0006. IBM SPSS was used for randomization, and the rats were grouped as follows: sham operation group (Sham group), model group (VD group), Bushenhuoxue formula

group (BSHX group), autophagy activator (rapamycin) group (Rap group), and autophagy inhibitor (3-methyladenine) group (3-MA group), with $n = 10$/gp. The Ethics Committee of the Hebei Institute of Traditional Chinese Medicine approved the study (approval No. DWLL2019008).

2.7 Model preparation and administration

The rats in each group were deprived of food for 12 h and water for 4 h before surgery. Anesthesia was 2% pentobarbital sodium (40 mg/kg, i.p.). The VD group, BSHX group, Rap group, and 3-MA group were modeled by two-vessel occlusion (2-VO) [19]. The rats were fixed in the supine position, and the skin was cut isssn the middle of the neck. The bilateral common carotid arteries and the vagus nerve were visualized, but only the common carotid artery was ligated. The wound was then sutured. In the Sham group, the vagus nerve and the common carotid artery were visualized but not ligated. Intramuscular injection of gentamicin (CSPC Ouyi Pharmaceutical Co., Ltd., China, production approval: 068180304; Specification: 2 mL = 80 mg) was administered to combat the infection.

The rats in the Rap group and 3-MA group were administered drug intracerebroventricularly 30 min before surgery. After being anesthetized with 2% pentobarbital, the rats' heads were fixed in a stereotaxic apparatus (Stoelting, USA, 51700). A medial incision of the scalp was made to expose the skull. The coordinated used were –0.9 mm (bregma), 1.5 mm lateral, and –3.6 mm from the skull. Coordinates were marked, and small round burr holes were made with the help of a drill. Rapamycin (Shanghai Yuanye Biological Technology Co., Ltd., China. batch number: H03A10Y94335; Specification: 500 mg) was dissolved in dimethyl sulfoxide (DMSO) at a concentration of 8 ng/μL. The 3-MA (Shanghai Yuanye Biological Technology Co., Ltd., China. batch number: Y23O10C99335; Specification: 1 g) was dissolved in normal saline at a concentration of 10 mmol/L. Rapamycin solution (4 μL) or 3-MA solution (6 μL) was delivered in a microliter Hamilton syringe through the hole at a rate of almost 1 μL/min. After injection of the drug, the syringe was kept in place for 5 minutes to avoid any injected substance loss. The rat was then taken out of the apparatus, and the wound was disinfected and sutured.

On day 3 after surgery, the BSHX group received an intragastric administration of 10.14 g/kg Chinese medicine 1×/day for 28 days; the remaining groups were given the same volume of normal saline every day. The composition of BSHXF was as follows: *Polygonum Multiflorum*, 15 g; *Alpiniae Oxyphyllae,* 15 g; *Juglans Regia L,* 15 g; *Panax Ginseng* C. A. *Mey*, 10 g; *Chuanxiong,* 15 g; *Radix Salvia,* 15 g; *Angelica Sinensis,* 15 g; and *Curcuma Aromatica Salisb*, 10 g. The solution was prepared proportionally to produce 1.014 g/mL, dissolved fully in distilled water, and refrigerated at 4 °C.

2.8 Morris water maze

The Morris water maze (MWM) (Beijing Zhongshidichuang Technology Co., Ltd., China, ZS-001) experiment was conducted 4 wk after surgery to test the rats' learning and memory abilities using a spatial-orientation task. MWM is a circular tank 160-cm in diameter and 50 cm deep. The tank was divided into four imaginary quadrants. In the third quadrant, a circular platform of 12-cm diameter and a height of 29 cm was hidden 1 cm below the water surface. The water temperature was maintained at between 22 °C and 25 °C. From days 1 to 5, a positioning navigation experiment was conducted. The rat was placed in the water and had to find the platform from the midpoint of each quadrant. The escape incubation period refers to the latency to board the platform and stay for 5 s. The rats that did not find the platform within the specified time were recorded as 120 s. On day 6, the space exploration experiment was conducted. We removed the platform and then put the rats into the water at any of the same entry points and recorded the number of times the rats crossed the original platform within 120 seconds to test the spatial memory ability of the rats.

2.9 Nissl staining

Three rats were taken from each group and given cardiac perfusion with 4% paraformaldehyde (Zhejiang Jinhua Top Health Biotechnology Co., Ltd. China, catalog No. 20170017). The brain was removed, fixed further in 4% paraformaldehyde, then conventionally embedded in paraffin. The wax block was trimmed to expose the hippocampus and then cut into coronal sections of 4-μm thickness. The tissue was then dewaxed and hydrated in xylene, gradient ethanol, and distilled water. After that, the tissue was stained in methylene blue for 10 min and underwent Nissl differentiation for color separation until the Nissl body was clear under the microscope. The slices were then placed into ammonium molybdate solution for 3–5 min, dehydrated, transparentized, and sealed routinely. Since the hippocampal CA1 region is most closely related to spatial discrimination and learning and memory, the pathological morphology of hippocampal CA1 in each group was observed under a digital microscope (Olympus Corporation, Japan, DP73), and the morphological changes and differences of Nissl-stained cells were observed and recorded at low and high magnification.

2.10 The ultrastructure of the hippocampus was observed by Transmission Electron Microscope (TEM)

After anesthesia, the rats in each group were decapitated, the hippocampi were stripped off on an ice platform, the tissue blocks of about 1 mm^3 were cut off with a scalpel in the CA1 region, placed in fixative for TEM (Wuhan ServiceBio Technologies Co Ltd., China, catalog No. G1102) for 2 h, washed with a phosphate-buffered solution for three times, and set in 1% osmic acid for 2 h. After cleaning three times with phosphate-buffer, the tissues were dehydrated in gradient ethanol, placed in acetone (Sinopharm Group Chemical Reagents Co., Ltd., China, catalog No. 10000418) three times, and soaked in a mixture of 1:1 and 1:2 acetone and EMBed 812 (SPI, USA, catalog No. 90529-77-4) for 1 h each. The tissue sections were then soaked in EMBed 812 for 4

h and sliced (thickness: 50 nm). After dual electron staining with uranium acetate and lead citrate, the image results were observed under TEM (HITACHI, Japan, HT7800) and recorded.

2.11 Western blot test

After anesthetization, the rats in each group were decapitated, and the hippocampal tissue was isolated on the ice platform and frozen in liquid nitrogen. The hippocampus was weighed, and 1 mL RIPA lysate (Shanghai Beyotime Biotechnology Co., Ltd., China, catalog No. P0013E) per 100 mg tissue was added. It was then cut into pieces, ground, centrifuged for 10 minutes, and the supernatant was taken for reserve. The protein concentration was adjusted to 6 μg/μL with lysate. The gel was prepared, and the glass plate was affixed to the electrophoresis apparatus (Beijing Liuyi Biotechnology Co., Ltd., China, DYY-III 7B). According to the quantitative results of the proteins, the total protein samples of the corresponding volume and 4$\times$ protein loading buffer was added and then denatured at 95 °C for 10 min. The electrophoretic solution was added to the sample included in each gel hole. The voltage was adjusted to 80V for 90 min and 120V when the sample was passed through the stacking and separation gel. The target band was run to about two-thirds of the separation gel position. Electrophoresis was stopped, and the glass plate was removed. The protein bands isolated from the gel were transferred onto the PVDF membrane (Pall Corporation, USA, catalog No. T22740) by transfer electrophoresis and then incubated with a specific primary antibody (LC3 antibody: CST, USA, catalog No. 12741. P62 antibody: NSJ Bio, China, catalog No. F48010. Beclin1 antibody: Abcam, UK, catalog No. Ab210498. GAPDH: Abcam, UK, catalog No. Ab9485) diluted to a 1:800 ratio, and then horseradish peroxidase-labeled secondary antibody (Beijing Zhongshan Jinqiao, catalog No. ZB2301) was added. Quantity One software (Bio-Rad Technical Service Department, USA) was used to measure the strip's gray value. The relative expression of the target protein was obtained by calculating the gray value ratio of the target protein and GAPDH. The relative expression of LC3 was defined as LC3-II/LC3-I ratio.

2.12 Statistical analysis

The data were analyzed and plotted using IBM SPSS 25.0 statistical software (IBM SPSS, IL, USA) and GraphPad Prism (Version 7.0, GraphPad Software, CA, USA). The results were presented as mean and standard deviation. One-way ANOVA was used to compare multiple groups that were normally distributed and had homogeneity of variance. The SNK test was used for data comparison between the two groups. A level of $p \leq 0.05$ was considered to be statistically significant for all hypothesis-testing methods.

3. Results

3.1 Prediction of co-target in BSHXF and VD

The active ingredients of *Panax Ginseng* C. A. *Mey*, *Angelica Sinensis*, *Chuanxiong Rhizoma*, *Curcuma Aromatica Salisb*, and *Radix Salviae* were searched in TCMSP and found (22, 2, 7, 15, and 65, respectively). The active ingredients of *Polygonum Multiflorum Thunb*, *Alpinia Oxyphylla Miq*, and *Juglans Regia L* were collected from TCMID and found (55, 33, and 30, respectively). A total of 229 active ingredients were obtained by combining the two databases. The main active ingredients information can be found in **Supplementary Table 2**. Target prediction was carried out for the above ingredients. After removing the repeated components, the data obtained were 105 in *Panax Ginseng* C. A. *Mey*, 29 in *Angelica Sinensis*, 18 in *Chuanxiong Rhizoma*, 34 in *Curcuma Aromatica Salisb*, and 394 in *Radix Salviae*. The target proteins were converted to corresponding gene symbols using the Perl and UniProt databases. Target prediction with the SwissTargetPrediction was made according to the probability of $>$0.11 screening. After removing the repeated ingredients, the data points obtained were 668 in *Polygonum Multiflorum Thunb*, 287 in *Alpinia Oxyphylla Miq* and 243 in *Juglans Regia L* (**Supplementary Table 3**). The targets of the above two databases were counted, and 502 potential targets were screened.

The disease genes were screened in GeneCards, OMIM, and DisGenet databases by searching for Vascular Dementia, Ischemic Vascular Dementia, and Vascular Dementia Acute Onset. In GeneCard and DISGENet, the screening criteria were set as relevance score $>$11.38 and DSI $\geq$0.5. Finally, all the data are merged and sorted out. The information from the three databases was integrated to obtain 601 disease genes. Finally, each drug-action target was compared with the disease target, and the co-action genes of the two were screened out. The Wayne map was drawn using the R language (Version 3.6.3, Lucent Technologies, USA) and Venny 2.1 (https://bioinfogp.cnb.csic.es/tools/venny/index.html) to obtain 95 intersecting genes that might lead to VD (**Supplementary Table 4**).

3.2 Construction and analysis of disease-drug PPI network and screening of core genes

According to the above filtering conditions, the data of the STRING database were used to draw the optical network topology diagram by Cytoscape 3.6.0 software (National Resource for Network Biology, USA) (Fig. 1A). We input the obtained files into R language for calculation and obtained the bar diagram of the core target of the protein-interaction network (Fig. 1B). The larger the number on the strip, the greater the probability of becoming the core gene. According to the BetweennessCentrality, the ClosenessCentrality, and the Degree, the top 20 core genes were selected: AKT1; IL6; GAPDH; CASP3; TNF; VEGFA; APP; MAPK1; EGFR; PTGS2; SRC; MAPK8; MYC' NOS3; HSP90AA1; MMP9; ESR1; MMP2; ICAM1; and ACE.

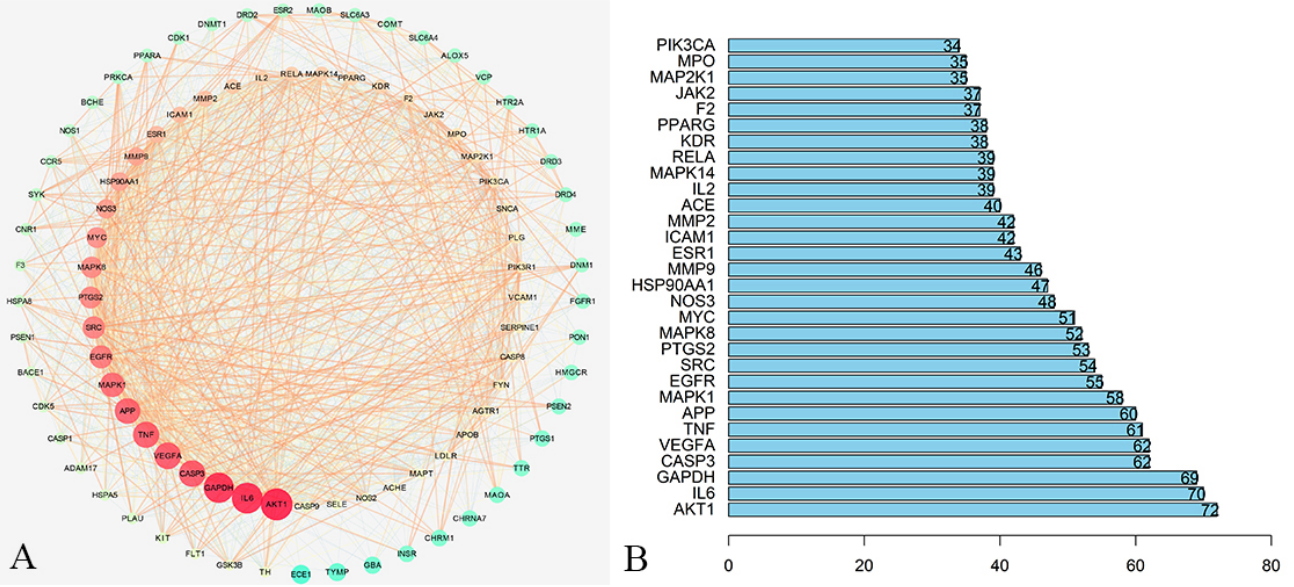

Fig. 1. The diagram of the core target of the protein interaction network. (A) The PPI visual network topology diagram of 95 common targets. The bigger the degree, the bigger the node, the darker the color, the more important the node. (B) The bar diagram of the top 30 core targets of the protein interaction network. On the left are the names of the genes. The number on the strip is the number of adjacent nodes of the corresponding gene.

3.3 Network construction of "traditional Chinese medicine-component-target-pathway" of BSHXF active ingredient-VD

The data were integrated, and Cytoscape 3.6.0 software was used to construct the visual network diagram of the "Traditional Chinese Medicine-component-target" of BSHXF-VD's active component. According to the results of network pharmacology and the visual topology diagram, we obtained the core compounds of 8 herbs in BSHXF (**Supplementary Table 5**). In the diagram, different targets correspond to the same active ingredient. A target can correspond to different ingredients, thus indicating that BSHXF has multi-component and multi-target VD treatment (Fig. 2).

3.4 GO biological process and KEGG pathway enrichment analysis of BSHXF

We finally enriched 95 core targets in the GO and KEGG pathways. A total of 320 pathways were obtained, of which 158 belonged to GO processes and 162 belonged to KEGG pathways (**Supplementary Tables 6,7**). The first 20 pathways with $p < 0.05$ were visualized through R language (R3.6.3). As shown in the figures, the GO biological functions of BSHXF in VD treatment involve endopeptidase activity, protein tyrosine kinase activity, growth factor receptor binding, protein serine/threonine kinase activity, G protein-coupled amine receptor activity, neurotransmitter binding. The KEGG enrichment pathway of BSHXF in the treatment of VD included the pathways of neurodegeneration - multiple diseases, PI3K-Akt signaling pathway, MAPK signaling pathway, HIF-1 signaling pathway (Figs. 3,4). Then, we used the core pathways to build the herb pathway-target network, as presented in Fig. 5.

3.5 Comparison of behavioral changes in Morris water maze tests in rats

The results of the position-navigation experiment revealed that compared with the Sham group, the escape latency of rats in the VD group, Rap group, and 3-MA group were shown to be longer ($p < 0.05$). Compared with the VD group, the escape latency of rats in the BSHX group was significantly shorter, and the difference was statistically significant [F (5, 49) =7.802, p = 0.000]. The results of the space-exploration experiment revealed that compared with the Sham group, the number of times the rats crossed the original platform in the VD group and Rap group was decreased, and compared with the VD group, the number of times rats crossed the original platform was increased, showing a statistically significant difference [F (5, 49) =13.62, p = 0.000] (Fig. 6).

3.6 Comparison of pathological morphology of rat hippocampus

Microscopic observation showed that the morphology and the structure of neurons in the hippocampal CA1 area of Sham group rats were as expected, the cells were orderly arranged, the nucleoli were apparent, and the number and volume of Nissl bodies were large. In the VD group and Rap group, the cells in the CA1 area were significantly damaged, with a sparse and disordered arrangement, and were irregular in shape. The nucleolus was compact or absent, and the Nissl bodies were absent. The morphology and the number of cells in the BSHX and 3-MA groups were less abnormal than those in the VD group. The cell space in the 3-MA group was enlarged and partially lost, and the Nissl bodies could be observed. The cells in the BSHX group were more orderly, and there were more Nissl bodies (Fig. 7).

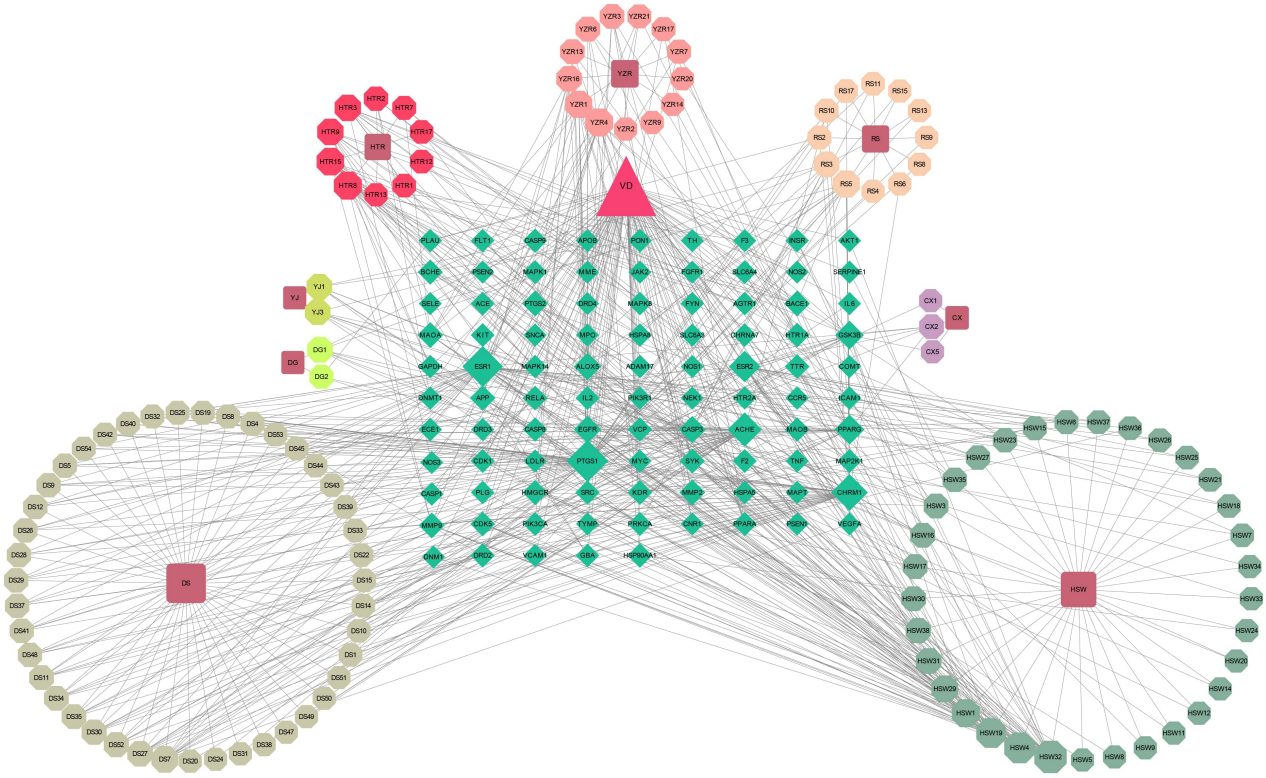

Fig. 2. Network of BSHXF-component-target. The octagon represents the compound target of the drug, the triangle represents the disease, and the diamond represents the disease target.

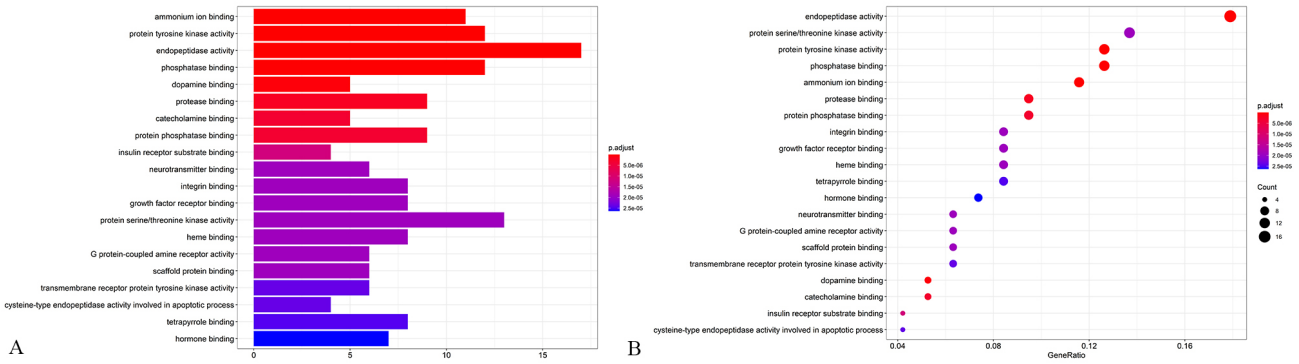

Fig. 3. The diagrams of GO functional-enrichment analysis. (A) The histogram of GO functional-enrichment analysis. The letters on the left of the graph are the names of GO biological functions, and the numbers below are the number of genes enriched on GO. The bar graph represents the biological functions enriched on GO, and *p* represents the significance of enrichment. The redder the color, the higher the degree of enrichment, and the smaller the corresponding *p*-value. (B) The bubble diagram of GO functional-enrichment analysis. The principle is the same as the histogram.

3.7 Comparison of ultrastructure observation of hippocampal neurons in rat brain

TEM observation revealed that the cells in the Sham group appeared normal in morphology and complete in structure, but no autophagy was observed. The VD group and Rap group cells were characterized by abnormal cell structure, nucleolus shrinkage and deformation, reduced mitochondrial number, and endoplasmic reticulum fracture. Autophagic lysosomes were observed intracellularly. The BSHX group and 3-MA group's cell morphology was better than that of the VD group. The organelle was relatively complete, the chromatin distribution was more uniform, and the autophagosomes were rare. The overall degree of cell damage from heavy to light was as follows: the VD group, the Rap group, the 3-MA group, the BSHX group, and the Sham group (Fig. 8).

3.8 Comparison of expression levels of autophagy-related protein in rats

The experiment was repeated 3 times, and there were no differences. Compared with the Sham group, the expres-

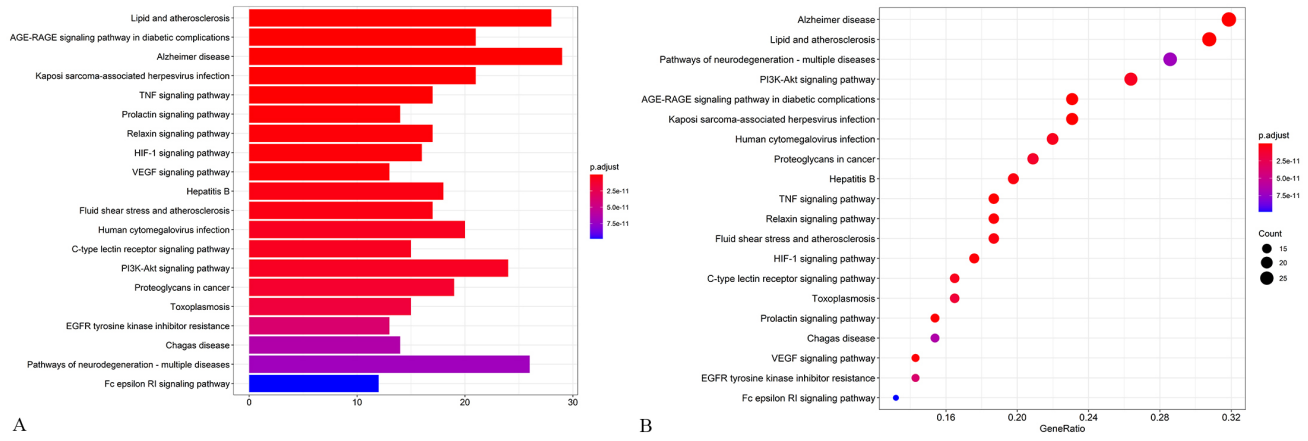

Fig. 4. The diagrams of KEGG pathway enrichment analysis. (A) The histogram of KEGG pathway enrichment analysis. The letters on the left of the graph are the names of KEGG pathways, and the numbers below are the number of genes enriched on KEGG. The bar graph represents the pathways enriched on KEGG, and p represents the significance of enrichment. The redder the color, the higher the degree of enrichment, and the smaller the corresponding p-value. (B) The bubble diagram of KEGG pathway enrichment analysis. The principle is the same as the histogram.

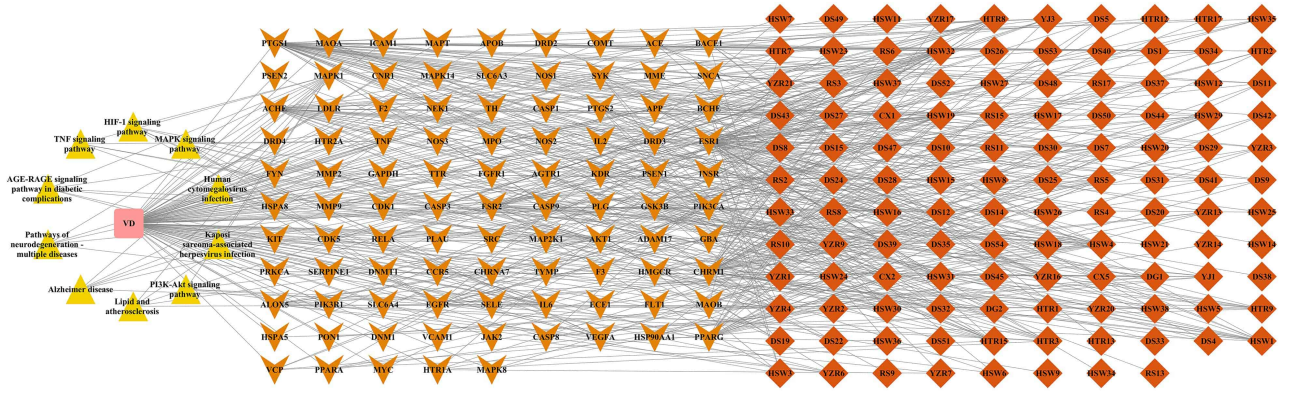

Fig. 5. Herb-pathway-targets network. The diamond represents the compound target of the drug, the triangle represents the pathway, and the arrowhead represents the disease target.

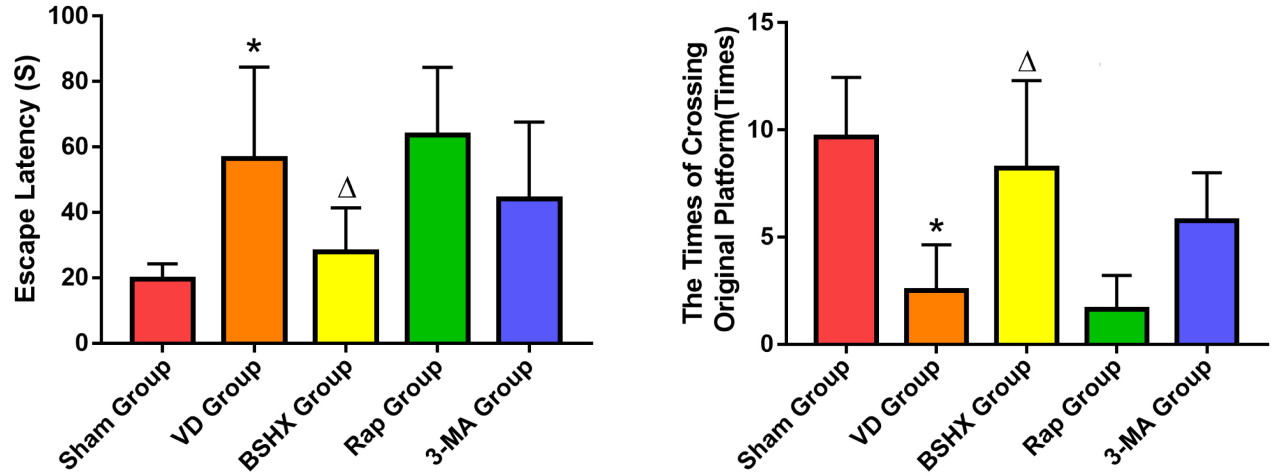

Fig. 6. The comparison of behavioral changes of Morris Water Maze in Rats. (A) The comparison of escape latency in rats. Compared with the Sham group,$^{*}p < 0.05$; Compared with the VD group, $^{\triangle}p < 0.05$. (B) The comparison of the times crossing the original platform in rats. Compared with the Sham group,$^{*}p < 0.05$; Compared with the VD group,$^{\triangle}p < 0.05$.

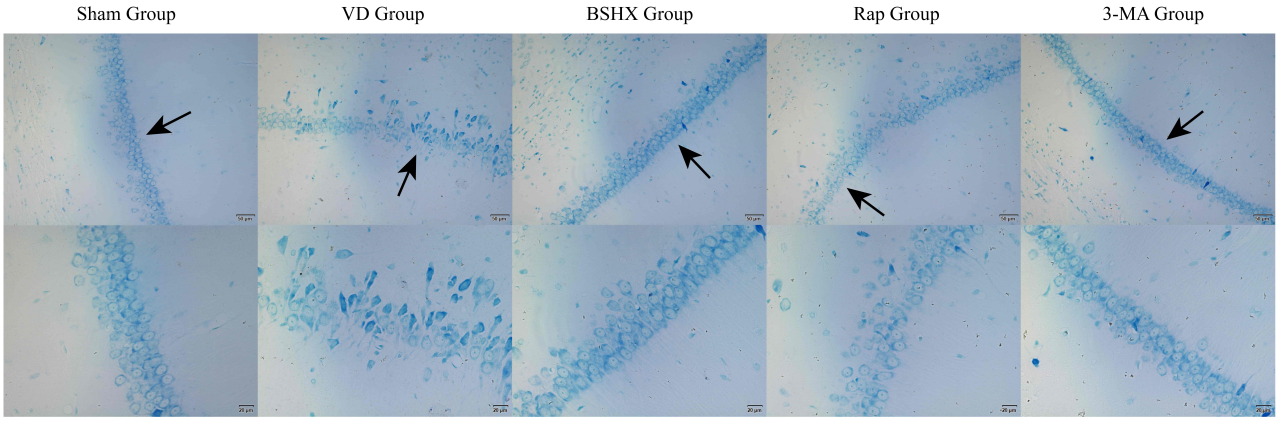

Fig. 7. Pathological morphology of hippocampal CA1 region of rats in each group. Each group had two views, one at low power (200×), and the other at high power (400×).

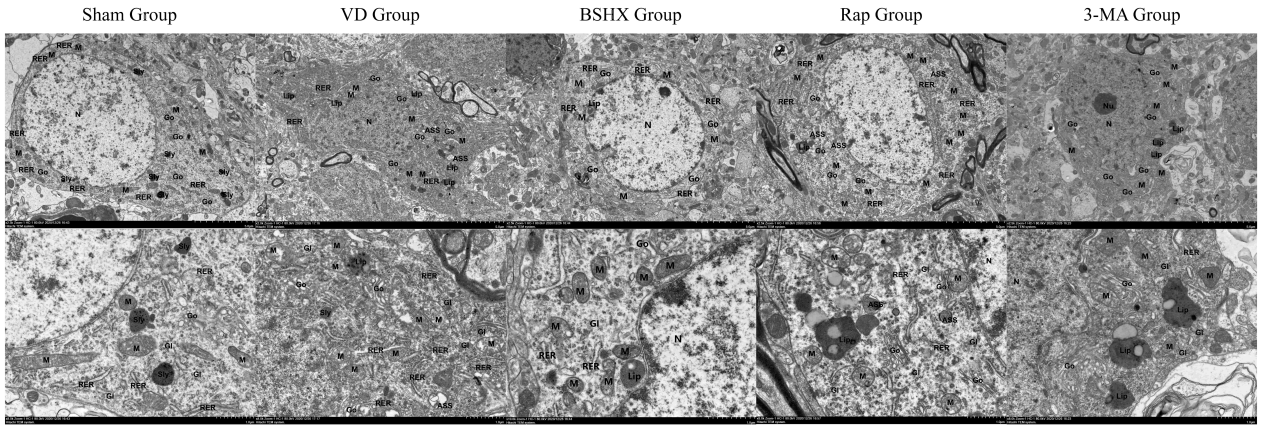

Fig. 8. Neuronal damage and autophagy in the hippocampal CA1 region of rats in each group were observed by TEM. Each group had two views, one at low power (2500×), and the other at high power (6000×). In the Sham group, the nuclei (N) were large and round, with abundant organelles, slightly damaged mitochondria(M), abundant secondary lysosomes (SLy). Rough endoplasmic reticulum (RER) was slightly dilated, surface ribosomes were degranulated, Golgi bodies (GO) were abundant, and glycogen (Gl) was evenly dispersed in the cells. No autophagy was observed in the cells (0). In the VD group, the nuclei were abnormal, the cells were irregular, there was more lipofuscin (Lip) and secondary lysosome accumulation in the cells, mitochondria were slightly vacuolated, and autophagic lysosomes (ASS) were observed intracellular (2). In the BSHX group, the nuclei were large and translucent, with abundant organelles, moderate mitochondrial edema, and no autophagy was observed (0). The RAP group had abnormal nuclei, irregular cells, more lipofuscin in cells, slight mitochondrial vacuolation, and more autophagy (3). In the 3-MA group, the nuclei were abnormal, and the cell body was slightly irregular. There was a certain amount of lipofuscin and a small number of secondary lysosomes in the cells. Mitochondria were slightly damaged, and no autophagy was observed (0).

sion levels of Beclin-1 and LC3 in the VD group and Rap group were increased, whereas the expression of P62 was decreased, and the difference was statistically significant [F (5, 19) = 18.064, p = 0.000]. Compared with the VD group, the expression of Beclin-1 and LC3 in the BSHX group and 3-MA group was lower. In contrast, the expression of P62 was greater, showing a statistically significant difference [F (5,19) =12.699, p = 0.000] (Fig. 9).

4. Discussion

According to the PPI network diagram, among the main targets of BSHXF for VD treatment, protein kinase B (Akt) is the downstream target protein of phosphatidylinositol 3-kinase (PI3K). The signaling pathway constituted by the two involves a classical anti-apoptotic and pro-survival signal-transduction pathway that regulates autophagy by activating the downstream target protein of rapamycin (mTOR) [20]. CASP-3 is one of the most well-known markers of apoptosis. Activation of CASP-3 leads to up-regulation of genes related to angiogenesis and down-regulation of genes related to pro-apoptotic pathways [21]. Few studies have revealed the unified mechanism of metabolic control of intracellular vascular endothelial growth factor A (VEGFA). The VEGFR2-AMPK-PEG3 axis is speculated to integrate core proteogly-

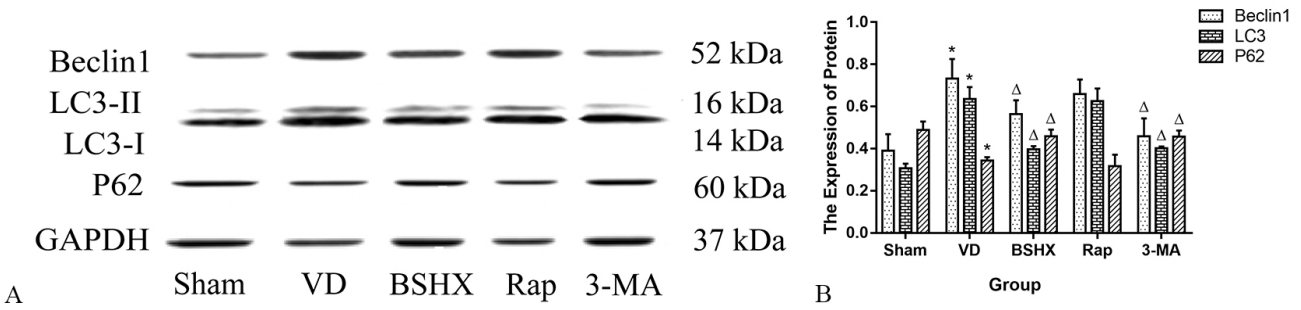

Fig. 9. Comparison of the expression levels of autophagy-related protein in rats. (A) The diagram of the western blot. (B) The diagram of expressions of autophagy-related protein. [Mean (SD), $n = 4$]. Compared with the Sham group,$^{*}p < 0.05$; Compared with the VD group,$^{\triangle}p < 0.05$. The red columns represent Beclin1/GAPDH, and the green columns represent LC3-II/LC3-I and P62/GAPDH.

can's anti-angiogenic and autophagic activities, which form the molecular basis of tumor inhibition [22]. The inhibition of MAPK and activation of NF-κB can reduce cerebral ischemia-reperfusion injury and improve neuropathies caused by reperfusion injury [23].

The KEGG pathway enrichment results showed that the PI3K-Akt signaling pathway is a classical anti-apoptotic and pro-survival pathway in various tissues and cells and has a protective effect on ischemia and hypoxia injury. Our previous study found that BSHXF could regulate PI3K/Akt pathway mediated by the brain-derived neurotrophic factor (BDNF), reduce neuronal damage, and relieve learning and memory impairment of VD rats [24]. Mitogen-activated protein kinase (MAPK) signaling pathway is a common and highly conserved mechanism in eukaryotic cell regulation [25]. Studies have shown that the MAPK family can regulate apoptosis, differentiation, inflammation, proliferation, and other stress induction factors [26, 27], and the MAPK signaling pathway showed association with neurodegenerative diseases [28]. The hypoxia-inducible factor HIF-1 signaling pathway (HIF-1 signaling pathway) acts as the vital transduction pathway of cellular response to hypoxia during cerebral ischemia. HIF induces BNIP3 and NIX genes that belong to BH3-only pro-apoptotic family members in the Bcl-2 family. The protein product can bind to the Bcl-2 gene competitively with Beclin-1, enabling Beclin-1 to dissociate and promote autophagy [29]. The results of our network pharmacology show that BSHXF activity is closely related to the PI3K/AKT signal pathway and that PI3K/AKT/mTOR is its downstream signal pathway, which is related to autophagy. Therefore, animal experiments with autophagy were conducted as the entry point to further verify the autophagy mechanism of BSHXF by regulating neuronal injury in the hippocampal region of VD rats.

Autophagy is a specific degradation process of protein and organelles in eukaryotic cells. Under pathological conditions, the regulation of autophagy can make cells better tolerate starvation, hypoxia, ischemia, and other stressful conditions [30]. By observing the brain's rat behavior and pathological morphology, rats' learning and memory abilities in the VD group decreased after cerebral ischemia significantly, and autophagy appears simultaneously as nerve cell damage. Further activation of autophagy in the Rap group could not alleviate neuronal damage and dementia in rats. The learning and memory abilities of rats in the BSHX group were improved significantly, and the neurons were repaired and regenerated. The 3-MA group also showed similar effects by autophagy inhibition.

As a critical factor of autophagy, Beclin-1 is involved in the formation of the autophagosomal separation membrane. The UNC-51-like kinase 1 complex and the type III PI3K complex can jointly mediate phosphorylation and aggregation of transmembrane protein Atg9 and promote aggregation of lipids and Atg proteins in the cytoplasm form a separation membrane [31]. Meanwhile, Beclin-1, a homologous related protein of yeast autophagy gene Atg6, forms a complex with PI3K to promote the formation of autophagosome membrane, recruit lipid molecules and other Atg proteins to locate on the autophagosome membrane, and play a positive regulatory role in the initiation of autophagy [32]. LC3 participates in the extension stage of the autophagosomal membrane. There are two ubiquitin-like binding effects, the ubiquitin-like binding of Atg12 to Atg5 and the ubiquitin-like binding of LC3-I to phosphatidylethanolamine [33]. When autophagy induction occurs, Atg7 can specifically activate the water-soluble LC3-I exposed to glycine residues at the C-terminal and bind phosphatidyl ethanolamine under the catalysis of Atg3 to form fat-soluble LC3-II. LC3-II is located on the inner and outer membranes of the autophagosome and is involved in the extension of the autophagosomal membrane and fuse with other membrane structures. Therefore, the LC3-II/LC3-I ratio is often used to indicate autophagic activity, and the protein level is directly proportional to the number of autophagosomes [34]. Ubiquitin-binding protein P62 is a stress-inducing protein that regulates several critical signaling pathways. It is involved in selective autophagy and is considered an essential indicator in detecting autophagy [35]. P62 can combine with LC3 to form a complex involved in forming autophagosomes and degradation of lysosomes through the N-terminal PB1 domain by

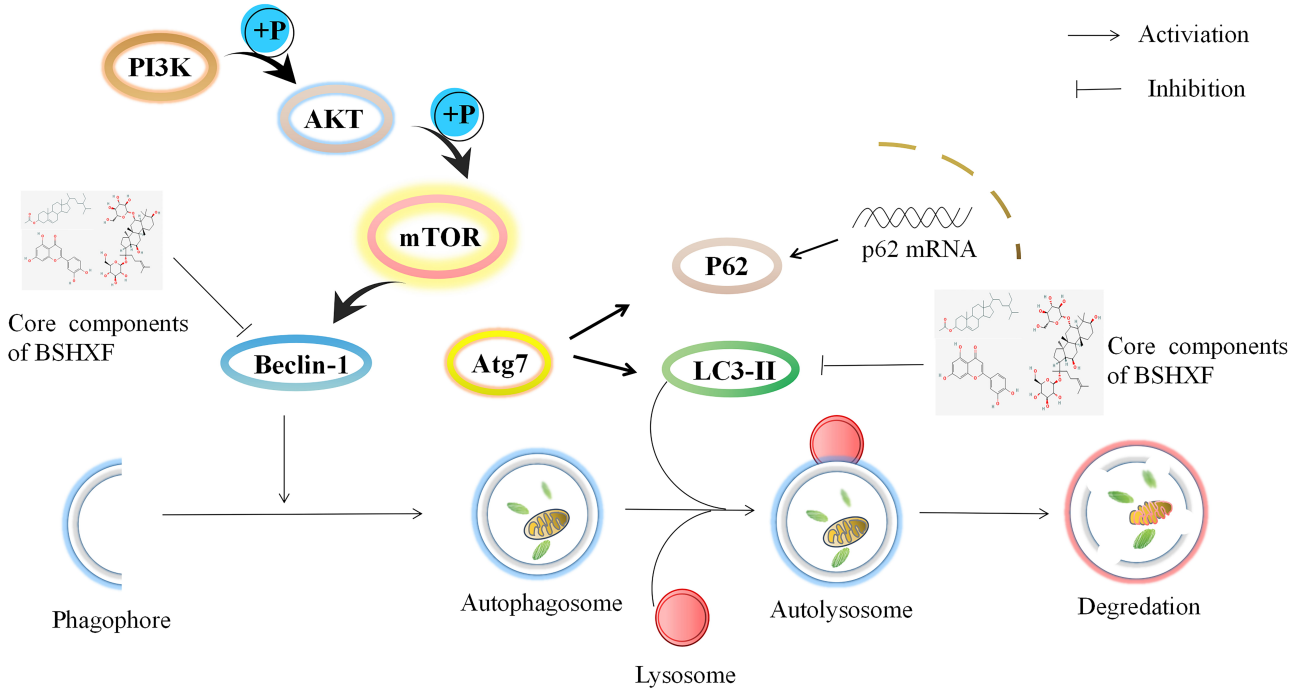

Fig. 10. Schematic diagram of the action mechanism of the core compounds related to autophagy in BSHXF. Core components of BSHXF inhibit autophagy during VD treatment. Its mechanism is closely related to the decrease of Beclin-1 and LC3 protein expression and increase of P62 expression in the hippocampus.

binding to LC3-II and accelerating the removal of protein aggregates [36]. Autophagy is shown to be associated with down-regulation of P62 expression, and its expression was negatively correlated with autophagy level [37].

Rapamycin was selected as an autophagy activator in this study, and its mechanism of action involves the promotion of autophagy by reducing the mTOR activity. As an autophagy inhibitor, 3-MA inhibits Class III PI3K to reduce the formation of autophagosomes. Both drugs are currently recognized and widely used as autophagy-intervention agents [38]. Western blotting results showed that compared with the Sham group, the protein expression levels of Beclin-1 and LC3 were significantly greater in the VD group and Rap group. In contrast, the P62 expression was lower. This indicated that the pathogenesis of VD was accompanied by autophagy, and activation of autophagy does not reduce brain damage and even aggravates the symptoms of VD rats. Compared with the VD group, the protein expression levels of Beclin-1 and LC3 in the BSHX group and 3-MA group were significantly higher, whereas P62 expression was lower. This indicated that TCM-gavage treatment down-regulates the autophagy level, and the effects were closely related to 3-MA. These results suggest that BSHXF inhibits autophagy during VD treatment. Its mechanism is closely related to the decrease of Beclin-1 and LC3 protein expression and increase of P62 expression in the hippocampus.

According to the research results, we found that many core components of BSHXF are related to autophagy. β-sitosterol can inhibit the proliferation and promote the apoptosis of gastric cancer cells. Its anticancer mechanism may be related to the autophagy induced by β-sitosterol through PI3K/AKT/mTOR pathway [39]. Luteolin has a significant protective effect on oxidative stress injury after cerebral ischemia-reperfusion. It can promote the degradation of mitochondrial autophagosomes and accelerate the clearance efficiency of ROS by improving the process of autophagy flow. Tanshinone II induces cell-cycle arrest by upregulating autophagy in human non-small cell lung cancer A549 cells, inhibiting cell proliferation and promoting the anti-tumor effect [40]. Resveratrol can significantly inhibit renal epithelial-mesenchymal cell transformation and alleviate renal interstitial fibrosis in diabetic mice, and its mechanism may be related to the promotion of renal autophagy [41]. The results suggest that ginsenoside Rg1 can delay premature ovarian failure induced by D-galactose through the PI3K/Akt/mTOR autophagy signal pathway. Other active ingredients that do not target autophagy may regulate the TGF-β/Smad pathway and the expression of inflammatory factors, reducing cytotoxicity by suppressing hepcidin expression in MES23.5 cells suppresses colorectal cancer cell growth by inhibiting the mTOR pathway *in vitro* and *in vivo* [42–44].

Traditional Chinese medicine has accumulated thousands of years of experience in the treatment of dementia. Modern studies have also shown that many traditional Chinese medicines have neuroprotective effects [45]. In the clinic, TCM has been widely used because of its minor side effects, prolonging the survival time of patients and improving the

quality of life of patients. In our study, network pharmacology suggests that many components of BSHXF are closely related to autophagy. Animal experiments have proved that BSHXF can play a neuroprotective role by inhibiting excessive autophagy. Some studies have shown that TCM extracts can alleviate renal aging by regulating autophagy. Treating neurodegenerative diseases with TCM extracts showed that diseases could be treated by regulating autophagy [46–48]. Therefore, in future research, the core components of BSHXF may be used as autophagy inhibitors combined with drugs through the regulation of autophagy to play a therapeutic advantage, to provide more possibilities for clinical treatment of VD.

The action mechanism of the core compounds related to autophagy in BSHXF is proposed in Fig. 10. BSHXF inhibited the expression of autophagy, but whether this result inhibited the formation of autophagosome or accelerated the degradation of autophagosome needs further dynamic monitoring and research. Moreover, whether there are interactions among the active component in BSHXF has not been studied, but we hope it will be included in research in the future.

5. Conclusions

We explored the molecular mechanism of BSHXF in the treatment of VD, analyzed and summarized the complex components and mechanism of action of BSHXF, and revealed the multi-target, multi-system, and multi-pathway regulatory effects of BSHXF on VD. The results showed that the occurrence of autophagy accompanied the pathogenesis of VD, and BSHXF could reduce the expression of Beclin-1 and LC3 in the hippocampus of VD rats, improve the expression of P62, reduce the damage of nerve cells and improve the learning and memory abilities by inhibiting the occurrence of excessive autophagy.

Abbreviations

BSHXF, Bushenhuoxue Formula; VD, vascular dementia; VCI, vascular cognitive impairment; TCM, traditional Chinese medicine; ADLs, activities of daily living; PI3K, Phosphoinositide 3-kinase; MAPK, mitogen-activated protein kinases; AKT1, Protein KinaseB; IL6, Inter Leukin-6; GAPDH, Glyceraldehyde phosphate dehydrogenase; CASP3, Cysteine-aspartate protease 3; TNF, Tumor Necrosis Factor; VEGFA, Vascular Endothelial Growth Factor; APP, Amyloid Precursor Protein; MAPK1, Mitogen-Activated Protein Kinases 1; EGFR, Epidermal Growth Factor Receptor; PTGS2, Prostaglandin endoperoxide synthase; SRC, Sarcoma virus-related genes; MAPK8, Mitogen-Activated Protein Kinases 8; MYC, Proto-oncogene; NOS3, Nitric oxide synthase; HSP90AA1, Human recombination protein; MMP9, Matrix metalloproteinase 9; ESR1, Estrogen receptor 1; MMP2, Matrix metalloproteinase 2; ICAM1, Intercellular adhesion molecule 1; ACE, Angiotensin-converting enzyme; KEGG, Kyoto; GO, Gene Ontology; Rap, rapamycin; 3-MA, 3-methyladenine; 2-VO, two-vessel occlusion; TEM, Transmission Electron Microscope; LC3, Microtubule-associated protein light chain 3; P62, sequestosome1; mTOR, Mechanistic target of rapamycin; CASP-3, caspase-3; BDNF, brain-derived neurotrophic factor.

Author contributions

SL and JJ performed the experiments, analyzed the data, prepared the figures and/or tables, and approved the final draft. YZ designed the experiments. WY and WG have discussed the results, authored or reviewed the drafts of the paper.

Ethics approval and consent to participate

Animals were raised and handled at the Laboratory Animal Center of the Hebei University of Chinese Medicine. The experimental animals involved in the research content and process of the project were following the relevant national requirements for medical laboratory animals and were approved by the Ethics Committee of Hebei College of Traditional Chinese Medicine (No. DWLL2020079).

Acknowledgment

We thank Xiuchao Geng for excellent criticism of the article.

Funding

This study was partially supported by the National Natural Science Foundation of China (No. 81873035), the Hebei Province Natural Science Fund (No. H2020423042), the Hebei Provincial Department of Education Science and Technology Research Key Funding Project (No. ZD2018009), and the Research Capacity Enhancement Project of Hebei University of Chinese Medicine (No. 2019-11).

Conflict of interest

The authors declare no conflict of interest.

Supplementary material

Supplementary material associated with this article can be found, in the online version, at https://www.imrpress.com/journal/JIN/20/4/10.31083/j.jin2004087.

References

[1] Cahill S. Who's global action plan on the public health response to dementia: some challenges and opportunities. Aging & Mental Health. 2020; 24: 197–199.

[2] Gorelick PB, Scuteri A, Black SE, Decarli C, Greenberg SM, Iadecola C, *et al.* Vascular contributions to cognitive impairment and dementia: a statement for healthcare professionals from the american heart association/american stroke association. Stroke. 2011; 42: 2672–2713.

[3] Strub R. Vascular Dementia. Southern Medical Journal. 2003; 96: 363–366.

[4] Skrobot OA, Black SE, Chen C, DeCarli C, Erkinjuntti T, Ford GA, *et al.* Progress toward standardized diagnosis of vascular cognitive impairment: Guidelines from the Vascular Impairment of

Cognition Classification Consensus Study. Alzheimer's & Dementia. 2018; 14: 280–292.
[5] Weekman EM, Sudduth TL, Caverly CN, Kopper TJ, Phillips OW, Powell DK, *et al.* Reduced Efficacy of Anti-a Immunotherapy in a Mouse Model of Amyloid Deposition and Vascular Cognitive Impairment Comorbidity. Journal of Neuroscience. 2016; 36: 9896–9907.
[6] Wu Y, Zhou Q, Zhang T, Li Z, Chen YP, Zhang P, *et al.* Discovery of Potent, Selective, and Orally Bioavailable Inhibitors against Phosphodiesterase-9, a Novel Target for the Treatment of Vascular Dementia. Journal of Medicinal Chemistry. 2019; 62: 4218–4224.
[7] O'Brien JT, Thomas A. Vascular dementia. Lancet. 2015; 386: 1698–1706.
[8] Wang W, Yu W, Nie J, Lan C, Zhang M. Characteristics of TCM Syndrome in Patients with Vascular Dementia. Journal of Basic Chinese Medicine. 2017; 23: 514–517+548.
[9] Wang Z. Liu S, Yu W. Clinical observation on 86 cases of vascular dementia treated by tonifying kidney and activating blood circulation. Chinese Journal of the Practical Chinese with Modern Medicine. 2005; 18: 1115–1116.
[10] Wang W, Zhang Y, Yu W, Gao W, Shen N, Jin B, *et al.* Bushenhuoxue improves cognitive function and activates brain-derived neurotrophic factor-mediated signaling in a rat model of vascular dementia. Journal of Traditional Chinese Medicine. 2020; 40: 49–58.
[11] Jin H, Yu W, Liu X, Li Q, Xu H, Zhang H, *et al.* Effect of Bushen Huoxue Formula on Hippocampal Cells Apoptosis and ERK2, CREB Expression in Rats with Vascular Dementia. Chinese Journal of Experimental Traditional Medical Formulae. 2018; 24: 129–135.
[12] Chong ZZ, Shang YC, Wang S, Maiese K. A Critical Kinase Cascade in Neurological Disorders: PI 3-K, Akt, and mTOR. Future Neurology. 2012; 7: 733–748.
[13] Luo T, Lu Y, Yan S, Xiao X, Rong X, Guo J. Network Pharmacology in Research of Chinese Medicine Formula: Methodology, Application and Prospective. Chinese Journal of Integrative Medicine. 2020; 26: 72–80.
[14] Guo W, Huang J, Wang N, Tan H, Cheung F, Chen F, *et al.* Integrating Network Pharmacology and Pharmacological Evaluation for Deciphering the Action Mechanism of Herbal Formula Zuojin Pill in Suppressing Hepatocellular Carcinoma. Frontiers in Pharmacology. 2019; 10: 1185.
[15] Waman VP, Sen N, Varadi M, Daina A, Wodak SJ, Zoete V, *et al.* The impact of structural bioinformatics tools and resources on SARS-CoV-2 research and therapeutic strategies. Briefings in Bioinformatics. 2021; 22: 742–768.
[16] Barshir R, Fishilevich S, Iny-Stein T, Zelig O, Mazor Y, Guan-Golan Y, *et al.* GeneCaRNA: a Comprehensive Gene-centric Database of Human Non-coding RNAs in the GeneCards Suite. Journal of Molecular Biology. 2021; 433: 166913.
[17] Amberger JS, Bocchini CA, Scott AF, Hamosh A. OMIM.org: leveraging knowledge across phenotype–gene relationships. Nucleic Acids Research. 2019; 47: D1038–D1043.
[18] Piñero J, Ramírez-Anguita JM, Saüch-Pitarch J, Ronzano F, Centeno E, Sanz F, *et al.* The DisGeNET knowledge platform for disease genomics: 2019 update. Nucleic Acids Research. 2020; 48: D845–D855.
[19] Zhu H, Zhang J, Sun H, Zhang L, Liu H, Zeng X, *et al.* An enriched environment reverses the synaptic plasticity deficit induced by chronic cerebral hypoperfusion. Neuroscience Letters. 2011; 502: 71–75.
[20] Heras-Sandoval D, Pérez-Rojas JM, Hernández-Damián J, Pedraza-Chaverri J. The role of PI3K/AKT/mTOR pathway in the modulation of autophagy and the clearance of protein aggregates in neurodegeneration. Cellular Signalling. 2014; 26: 2694–2701.
[21] Bernard A, Chevrier S, Beltjens F, Dosset M, Viltard E, Lagrange A, *et al.* Cleaved Caspase-3 Transcriptionally Regulates Angiogenesis-Promoting Chemotherapy Resistance. Cancer Research. 2019; 79: 5958–5970.
[22] Neill T, Chen CG, Buraschi S, Iozzo RV. Catabolic degradation of endothelial VEGFA via autophagy. Journal of Biological Chemistry. 2020; 295: 6064–6079.
[23] Xie W, Zhu T, Dong X, Nan F, Meng X, Zhou P, *et al.* HMGB1-triggered inflammation inhibition of notoginseng leaf triterpenes against cerebral ischemia and reperfusion injury via MAPK and NF-κB signaling pathways. Biomolecules. 2019; 9.
[24] Wang W, Jin H, Geng X, Yu W, Wang X, Li Q, *et al.* Establishment of a rat model of vascular dementia with kidney deficiency and blood stasis syndrome. Journal of Basic Chinese Medicine. 2020; 26: 748–752.
[25] Kyriakis JM, Avruch J. Mammalian MAPK signal transduction pathways activated by stress and inflammation: a 10-year update. Physiological Reviews. 2012; 92: 689–737.
[26] Sun Y, Liu W, Liu T, Feng X, Yang N, Zhou H. Signaling pathway of MAPK/ERK in cell proliferation, differentiation, migration, senescence and apoptosis. Journal of Receptor and Signal Transduction Research. 2015; 35: 600–604.
[27] Guo G, Yao W, Zhang Q, Bo Y. Oleanolic acid suppresses migration and invasion of malignant glioma cells by inactivating MAPK/ERK signaling pathway. PLoS ONE. 2013; 8: e72079.
[28] Kim EK, Choi E. Compromised MAPK signaling in human diseases: an update. Archives of Toxicology. 2015; 89: 867–882.
[29] Glick D, Barth S, Macleod KF. Autophagy: cellular and molecular mechanisms. The Journal of Pathology. 2010; 221: 3–12.
[30] Mizushima N, Levine B, Cuervo AM, Klionsky DJ. Autophagy fights disease through cellular self-digestion. Nature. 2008; 451: 1069–1075.
[31] Papinski D, Schuschnig M, Reiter W, Wilhelm L, Barnes CA, Maiolica A, *et al.* Early steps in autophagy depend on direct phosphorylation of Atg9 by the Atg1 kinase. Molecular Cell. 2014; 53: 471–483.
[32] Guo F, Liu X, Cai H, Le W. Autophagy in neurodegenerative diseases: pathogenesis and therapy. Brain Pathology. 2018; 28: 3–13.
[33] Liu T, Yu J, Liu Y, Chen H, Kuang W, Wang X, *et al.* Effects of serum-free starvation on proliferative capacity of muscle satellite cells and expression of autophagy-related proteins LC3 and Beclin1. Chinese Journal of Tissue Engineering Research. 2019; 23: 1657–1661.
[34] Metlagel Z, Otomo C, Ohashi K, Takaesu G, Otomo T. Structural insights into E2-E3 interaction for LC3 lipidation. Autophagy. 2014; 10: 522–523.
[35] Jiang P, Mizushima N. LC3- and p62-based biochemical methods for the analysis of autophagy progression in mammalian cells. Methods. 2015; 75: 13–18.
[36] Li S, Jiang Z, Chai W, Xu Y, Wang Y. Autophagy activation alleviates nonylphenol-induced apoptosis in cultured cortical neurons. Neurochemistry International. 2019; 122: 73–84.
[37] Yang R, Song Z, Wu S, Wei Z, Xu Y, Shen X. Toll-like receptor 4 contributes to a myofibroblast phenotype in cardiac fibroblasts and is associated with autophagy after myocardial infarction in a mouse model. Atherosclerosis. 2018; 279: 23–31.
[38] Shi Z, Deng J, Fu S, Wang L, Wang Q, Liu B, *et al.* Protective effect of autophagy in neural ischemia and hypoxia: Negative regulation of the Wnt/β-catenin pathway. International Journal of Molecular Medicine. 2017; 40: 1699–1708.
[39] Sun Y, Liu X, Pian G. Study on the effect and mechanism of autophagy and apoptosis induced by β-sitosterol in human gastric cancer cells. Journal of Chinese Physician. 2019; 21: 866–871.
[40] Wen W, Hou X, Cui S, Shen C, Ye R, Cui Y, *et al.* Cell Cycle Arrest in A549 Cells Caused by Tanshinone IIA Induced Autophagy. Traditional Chinese Drug Research and Clinical Pharmacology. 2020; 31: 539–545.
[41] Zhao J, Zhang Y, Duan L, Zhao S, Ruan Y, Peng C, *et al.* Effect of resveratrol on autophagy and renal interstitial fibrosis in kidney of diabetic mice. Chinese Journal of Pathophysiology. 2020; 36: 893–898.

[42] Zhang H, Yi JK. Rhein Suppresses Colorectal Cancer Cell Growth by Inhibiting the mTOR Pathway *In Vitro* and *In Vivo*. Cancers. 2021; 13.
[43] Wang R, Wu G, Dai T, Lang Y, Chi Z, Yang S, *et al*. Naringin attenuates renal interstitial fibrosis by regulating the TGF-β/Smad signaling pathway and inflammation. Experimental and Therapeutic Medicine. 2021; 21: 66.
[44] Rivoira MA, Rodriguez V, Talamoni G, de Talamoni NT. New Perspectives in the Pharmacological Potential of Naringin in Medicine. Current Medicinal Chemistry. 2021; 28: 1987–2007.
[45] Wang Z, Chen B, Lin Y, Xing J, Wei Z, Ren L. Herbal decoction of Gastrodia, Uncaria, and Curcuma confers neuroprotection against cerebral ischemia in vitro and in vivo. Journal of Integrative Neuroscience. 2020; 19: 513-519.
[46] Liu H, Zhang Z, Zang C, Wang L, Yang H, Sheng C, *et al*. GJ-4 ameliorates memory impairment in focal cerebral ischemia/reperfusion of rats via inhibiting JAK2/STAT1-mediated neuroinflammation. Journal of Ethnopharmacology. 2021; 267: 113491.
[47] Zong W, Zeng X, Chen S, Chen L, Zhou L, Wang X, *et al*. Ginsenoside compound K attenuates cognitive deficits in vascular dementia rats by reducing the aβ deposition. Journal of Pharmacological Sciences. 2019; 139: 223–230.
[48] Liu B, Tu Y, He W, Liu Y, Wu W, Fang Q, *et al*. Hyperoside attenuates renal aging and injury induced by D-galactose via inhibiting AMPK-ULK1 signaling-mediated autophagy. Aging. 2018; 10: 4197–4212.